An effective sanitizer for fresh produce production: *In situ* plasma activated water treatment inactivates pathogenic bacteria and maintains the quality of cucurbit fruit

Running title: Efficacy of PAW as a fresh produce sanitizer

Joanna G. Rothwell[a], Jungmi Hong[b], Stuart J. Morrison[c], Heema Kumari Nilesh Vyas[b,d], Binbin Xia[b], Anne Mai-Prochnow[b], Robyn McConchie[a], Kim-Yen Phan-Thien[a], Patrick J. Cullen[b], Dee A. Carter[a,d,#]

[a]ARC Training Centre for Food Safety in the Fresh Produce Industry, School of Life and Environmental Sciences, Faculty of Science, Sydney Institute of Agriculture, The University of Sydney, Sydney, New South Wales, Australia

[b]School of Chemical and Biomolecular Engineering, The University of Sydney, Sydney, New South Wales, Australia

[c]Department of Agricultural and Resource Economics, University of California, Davis, California, USA

[d]Sydney Institute of Infectious Diseases, The University of Sydney, Sydney, New South Wales, Australia

[#]Address correspondence to Dee A. Carter, dee.carter@sydney.edu.au

Abstract

The effect of plasma activated water (PAW) generated with a dielectric barrier discharge diffusor (DBDD) system on microbial load and organoleptic quality of cucamelons was investigated and compared to the established sanitizer, sodium hypochlorite (NaOCl). Pathogenic serotypes of *Escherichia coli*, *Salmonella enterica,* and *Listeria monocytogenes* were inoculated onto the surface of cucamelons (6.5 log CFU g^{-1}) and into the wash water (6 log CFU mL^{-1}). PAW treatment involved 2 minutes *in situ* with water activated at 1500 Hz and 120 V, and air as the feed gas; NaOCl treatment was a wash with 100 ppm total chlorine; and the control treatment was a wash with tap water. PAW treatment produced a 3 log CFU g^{-1} reduction of pathogens on the cucamelon surface without negatively impacting quality or shelf life. NaOCl treatment reduced the pathogenic bacteria on the cucamelon surface by 3-4 log CFU g^{-1}, however, this treatment also reduced fruit shelf life and quality. Both systems reduced 6 log CFU ml^{-1} pathogens in the wash water to below detectable limits. The critical role of superoxide anion radical ($\cdot O_2^-$) in the antimicrobial power of DBDD-PAW was demonstrated through a scavenger assay, and chemistry modelling confirmed that $\cdot O_2^-$ generation readily occurs in DBDD-PAW generated with the employed settings.

Modelling of the physical forces produced during plasma treatment showed that bacteria likely experience strong local electric fields and polarization. We hypothesize that these physical effects synergise with reactive chemical species to produce the acute antimicrobial activity seen with the *in situ* PAW system.

Importance

Plasma activated water (PAW) is an emerging sanitizer in the fresh food industry, where food safety must be achieved without a thermal kill step. Here we demonstrate PAW generated *in situ* to be a competitive sanitizer technology, providing a significant reduction of pathogenic and spoilage micro-organisms while maintaining the quality and shelf life of the produce item. Our experimental results are supported by modelling of the plasma chemistry and applied physical forces, which show that the system can generate highly reactive superoxide radicals and strong electric fields that combine to produce potent antimicrobial power. *In situ* PAW has promise in industrial applications as it only requires low power (12 W), tap water and air. Moreover, it does not produce toxic by-products or hazardous effluent waste, making it a sustainable solution for fresh food safety.

Keywords

Fresh produce, cold plasma, cucurbitaceae, superoxide, antimicrobial treatment, food safety, *E. coli, Salmonella, Listeria,* spoilage

Introduction

Fresh fruit and vegetables are an important component of a healthy diet and are frequently eaten raw or with minimal processing. However, fresh produce can potentially become contaminated by microbes, including l human pathogens, during production and so post-harvest sanitizer treatments are therefore applied to reduce the risk of foodborne disease (1-4). Many types of fresh produce are treated with sanitizer washes to remove debris and reduce spoilage organisms adhered to the produce surface (5, 6). Sanitizers are also critical for reducing the risk of cross contamination by pathogens that may have been transferred into the wash solution (7-10).

Sanitizers containing active chlorine compounds such as sodium hypochlorite (NaOCl) are widely used in the post-harvest treatment of fresh produce. However, chlorine reacts with

soil and other organic compounds from the fruit and vegetables in the wash water leading to the formation of toxic chlorinated disinfection by-products (DBPs) (11). The creation of DBPs lowers the amount of free chlorine available for sanitation (12, 13) which may lead to survival and subsequent cross contamination of fresh produce with pathogenic bacteria (10). DBPs created from food sanitisationare also hazardous for workers in the processing environment and, are potentially carcinogenic (14-16). For Australian fresh produce to be certified as organic, chlorine sanitizers cannot be used (5), and globally there is an increasing trend for countries to eliminate their use in fresh produce production (17). This highlights the need for alternative sanitizer technologies that are better for the environment and consumers whilst also being effective in maintaining the safety and quality of fresh produce.

Cold atmospheric plasma is an emerging sanitizer technology with a variety of applications including in food production (18). Cold plasma is generated by applying electrical discharges to a gas so that orbital electrons are stripped from atoms, in a process called ionization. This results in a highly reactive mixture of excited species, free electrons, ions, and photons. Plasma gas can be discharged into water, which changes the physicochemical properties of the solution, and results in the generation of a large variety of reactive species, such as hydrogen peroxide (H_2O_2), nitrite ions (NO_2^-), nitrate ions (NO_3^-), superoxide anion radicals ($\cdot O_2^-$) and hydroxyl radicals (·OH) (19). The generated solution, called plasma activated water (PAW), has demonstrated antimicrobial power in the treatment of strawberries (20), blueberries (21), grapes (22), tomatoes (23) mushrooms (24) and leafy greens (25, 26). PAW technology represents a critically needed alternative to toxic chlorine-based sanitizers and it requires only air, tap water, a plasma generator, and electricity to run.

In order to apply PAW to fresh produce decontamination, it is important to consider the economic viability of technology destined for eventual scale-up and application in industrial processing. For example, current research frequently uses purified or distilled water as the PAW substrate (27, 28). However, tap water is more reflective of current (and potential future) industry practice, even though it may produce lower antimicrobial power and less reproducible results than purified or distilled water (29). Similarly, current PAW research frequently uses discharge gases such as argon or oxygen in plasma generation. These gases are expensive and unfeasible to use in fresh produce industries, which typically operate on

narrow profit margins (30). Produce shelf life and quality are important considerations for the food industry that may be influenced by PAW treatment, but these interactions have not yet been adequately assessed. Finally, PAW research needs to have compatibility with current process flows used in industry by reducing or maintaining sanitiser treatment times and by reducing or eliminating the need for additional steps such as pre-activation of the water.

In our previous work, we demonstrated rapid antimicrobial power against bacterial foodborne pathogens using a dielectric barrier discharge diffusor (DBDD) PAW system with tap water as the PAW substrate and air as the discharge gas (29). Physicochemical analysis of the PAW revealed that a DBDD reactor using tap water produced extremely low concentrations of reactive nitrogen species (NOx) and H_2O_2, and scavenger assays demonstrated that $\cdot O_2^-$ was essential for the antimicrobial activity of this system.

In the current study, we tested the efficacy of the DBDD-PAW system using cucamelons (*Melothria scabra)* as a fresh produce model. These are a type of cucurbit that produce small fruit similar in flavour and texture to cucumber, with skin resembling that of a watermelon. We compared DBDD-PAW with commercially relevant concentrations of NaOCl for its capacity to reduce bacterial pathogens while preserving cucamelon shelf life. To further investigate the unique antimicrobial properties of the *in situ* DBDD-PAW system, we simulated the local electric field distribution and polarization on bacterial cells in solution and on the cucamelon surface. Intense local electric fields are shown to contribute to the antimicrobial power of *in situ* PAW systems via membrane damage and electroporation (31). We hypothesise that $\cdot O_2^-$ and/or downstream reactive species combined with the membrane damage induced by electric fields and polarization lead to the antimicrobial activity observed in this system.

2. Materials and methods

2.1 Sanitizer and wash preparations

Three wash treatments were used in this study: a sterile tap water control, 100-ppm total chlorine NaOCl solution, and PAW. An untreated control, where cucurbits did not receive any washing, was also included. All treatments were made using autoclaved tap water cooled to 4 °C in a final volume of 200 mL. Concentrated NaOCl (Sigma-Aldrich) was diluted to 100 ppm (± 1 ppm) total chlorine using a Kemio^{TM} test kit with test sensors suitable for high range chlorine concentrations (Palintest, Tyne & Wear). The pH was adjusted to 6.5 ± 0.1 (SevenCompact S220, Mettler-Toldeo) using 10 % lactic acid. The PAW system configuration is illustrated in Figure 1. PAW was generated with a DBDD probe (PlasmaLeap Technologies, which has been described in detail previously (29). Power was supplied from a Leap100 micropulse generator (PlasmaLeap Technologies). The power supply settings used were 1500 Hz, 120 volts, 100 microseconds duty cycle, and 60 kHz resonance frequency. Compressed air was used as the processing gas at 1 standard litre per minute (SLM).

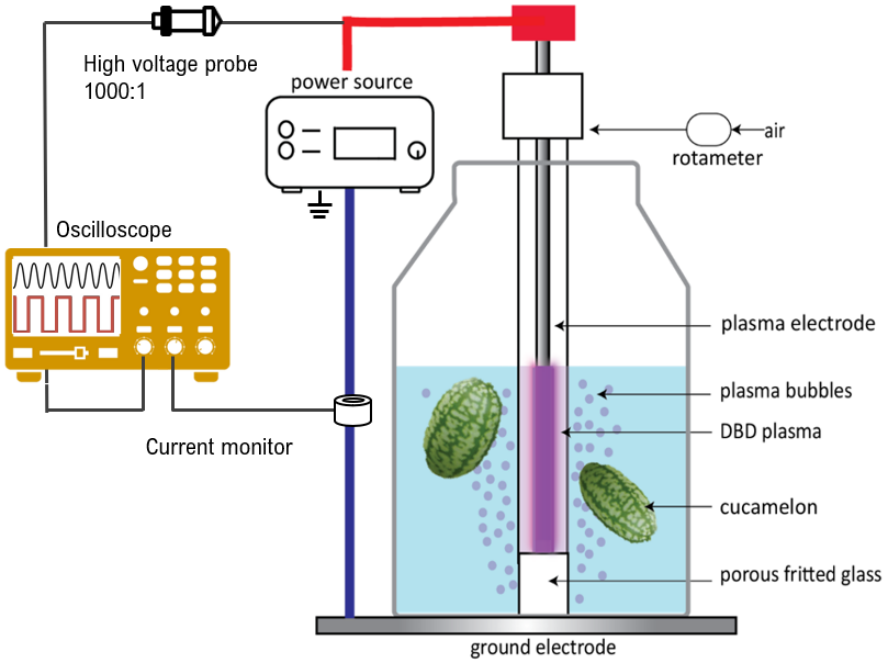

Figure 1. Schematic of the experimental design for the treatment of cucamelons by PAW generated by a dielectric barrier discharge diffusor (DBDD) system.

2.2 Bacterial culture preparation

The cultures listed in Table 1 were stored as glycerol stocks at -80 °C. Prior to experimentation, bacteria were resuscitated from frozen stocks by plating onto either

tryptic soy agar (TSA: 17 g L^{-1} pancreatic digest of casein, 5 g L^{-1} papaic digest of soybean meal, 5 g L^{-1} sodium chloride, 15 g L^{-1} agar-agar) for *S. enterica* and *E. coli* with incubation at 37 °C for 24 h, or tryptic soy sheep blood agar (TSBA: TSA with 5% defibrinated sheep's blood) for *L. monocytogenes* with incubation at 30 °C for 48 h. A single colony of each strain was then inoculated into separate tubes 10 mL of tryptic soy broth (TSB: 17 g L^{-1} pancreatic digest of casein, 2.5 g L^{-1} D(+) glucose monohydrate, 3 g L^{-1} papaic digest of soybean meal, 5 g L^{-1} sodium chloride, 2.5 g L^{-1} di-potassium hydrogen phosphate) for 18 h with shaking at 200 RPM at 37 °C for *S. enterica* and *E. coli* or 30 °C for *L. monocytogenes*. Cultures were centrifuged at 3000 RPM for 10 min at 4 °C, resuspended in phosphate-buffered saline (PBS, Oxoid), stored at 4 °C, and used within 4 h. Immediately prior to experimentation, equal volumes of the three strains of each species were mixed to create a 3-strain cocktail. Each cocktail was serially diluted in PBS, spread-plated, and incubated as above to determine the final inoculum concentrations.

Table 1. Bacterial isolates used in this study

Species	Strain designation	Serotype	Source (yr), details
Salmonella enterica subsp. *enterica*	ICPMR: 06-17- 184-1802	Saintpaul	Faeces (2017)
S. enterica subsp. *enterica*	ICPMR: 80-17-173-5603	Hvittingfoss	Faeces (2017), clustered with a 2016 rockmelon salmonellosis outbreak in Australia
S. enterica subsp. *enterica*	ICPMR: 80-17-149-5555	Anatum	Faeces (2017), clustered with a 2016 bagged salad product salmonellosis outbreak in Australia
Escherichia coli	ICMPR: 40-16-302-2227	O157:H7	Faeces (2016)
E. coli	ICPMR: 80-16-270-5374	O26:H11	Faeces (2016)
E. coli	ICPMR: 80-16-302-4575	O111:H-	Faeces (2016)
Listeria monocytogenes	ATCC: 51772; 3M:4395	1/2a	Cheese
L. monocytogenes	ICMPR: 80-13-220-4103	1/2b	Blood (2013), same binary type as 2010 fresh-cut melon listeriosis outbreak in Australia
L. monocytogenes	ICPMR: 80-18-038-5080	4bV	Blood (2018), clustered with a 2018 rockmelon listeriosis outbreak in Australia

2.3 Inoculation, treatment and microbial analysis of cucamelons

Fresh unwashed cucamelons were home grown harvested a day before experimentation. For each treatment condition, two cucamelons of similar size each weighing a total of 10 g (± 0.5 g) were selected. Cucamelons were first briefly immersed in 80% ethanol and rinsed with sterile tap water to reduce background microbial load. Each cucamelon was then spot-inoculated with ten x 10 mL of the *E. coli* or *S. enterica* inoculum at a final concentration of 1×10^9 colony forming units (CFU) mL^{-1}, or with twenty × 10 mL spots of *L. monocytogenes* at 8×10^8 CFU mL^{-1}, as this species has a lower adhesion to cucumber (32). Inoculated cucamelons were dried in a biosafety cabinet until there was no visible moisture remaining

(approximately 45 minutes). To simulate contaminated wash water, 200 mL of the inoculum was added to each of the 200 mL of treatment solutions along with the inoculated cucamelons. For the PAW condition, the cucamelons and contaminated wash solution were plasma treated for 2 minutes as described in section 2.1. To standardise the effect of the bubbling across the treatments, the DBDD probe was inserted into the water and bubbled without plasma generation for the control and NaOCl conditions.

Following treatment, the cucamelons were removed with sterile tweezers and placed into a stomacher filter bag with 40 mL of PBS and homogenised with a paddle blender (BagMixer 400, Interscience, France) for 2 minutes. An untreated control was included where inoculated cucamelons were homogenised without any wash treatment. 1 mL of cucamelon homogenate and 1 mL of the wash water were serially diluted with PBS and spread-plated onto TSA for *E. coli* and *S. enterica* or BA for *L. monocytogenes* and incubated as described in section 2.2 for enumeration of pathogens.

Our previous work had identified $\cdot O_2^-$ as a critical reactive species for the antimicrobial power of the DBDD-PAW (29). We investigated the antimicrobial role of $\cdot O_2^-$ in the fresh produce model by adding the $\cdot O_2^-$ scavenger tiron (Sigma-Aldrich) to the PAW system at a final concentration of 20 mM (33).

All experiments were performed in duplicate with biological triplicates performed on separate days. Cucamelons were harvested every fortnight across the season for each biological replicate. To identify significant differences between treatment groups, one-way ANOVA with Tukey's multiple comparison tests were performed using GraphPad Prism version 8.0.0 (GraphPad Software). A p-value of <0.05 was considered statistically significant.

2.4 Scanning electron microscopy

Scanning electron microscopy (SEM) was performed to evaluate morphological changes to bacterial cell structures after treatment with PAW, NaOCl, or the water control. Cucamelons were inoculated with *E. coli* or *L. monocytogenes* and treated as per section 2.3. Immediately after treatment, a sterile scalpel was used to slice 1-mm thick sections from

the cucamelon surface. The sections were placed into 2.5% glutaraldehyde fixative solution in 0.1 M phosphate buffer (pH 7) at room temperature for 1 h with gentle agitation and then stored at 4 °C. Samples were then washed with 0.1 M phosphate buffer 3 times for 5 minutes. The samples were then dehydrated using an ethanol concentration gradient with 2 washes for 5 minutes in 30, 50, 70, 80 and 90% ethanol followed by three 5-minute washes in 95 and 100% ethanol. Next, the samples were dried using critical point dying with liquid CO_2. Samples were then fixed to aluminium stubs with carbon tape and sputter coated with 10 nm of gold at 39 mA using a CCU-010 HV high compact vacuum coating system (Safematic, Switzerland). Samples were imaged using the Zeiss Sigma VP HD scanning electron microscope at 5 kV (ZEISS, Germany).

2.5 Shelf life and organoleptic quality assessment of cucamelons following treatment

The effects of each wash treatment on the background microflora, organoleptic quality, and shelf life of the cucamelons were assessed. For each of the four conditions, six cucamelons with no visible defects were selected. The cucamelons were treated with the sanitizers as described in Section 2.3 with the inoculation and ethanol rinse steps omitted. The cucamelons were then placed into 6 well plates (Corning Costar) and stored at 9 °C with 85% humidity (34). The following experiments were repeated across three biological replicates performed on different weeks.

2.6 Background microflora assessment

On day 0, 7, 14 and 21, two cucamelons from each treatment group were removed and stomached as described in section 2.3. 1 mL of the cucamelon homogenate was serially diluted in PBS, spread on plate count agar (PCA: enzymatic digest of casein 5 g L^{-1}, yeast extract 2.5 g L^{-1}, glucose 1 g L^{-1}, agar-agar 15 g L^{-1}) and incubated at 25 °C for 3 days to enumerate the total mesophilic aerobic bacteria. 1 mL of the cucamelon homogenate was also serially diluted in PBS, spread onto Dichloran Rose Bengal Chloramphenicol agar (DRBC, Oxoid), and incubated at 25 °C for 5 days to enumerate yeasts and moulds.

2.7 Texture analysis

The flesh firmess of the treated cucamelons was analyzed using TMS-Pro Texture analyser (Food Technology Corporation, Virginia, United States) fitted with a 3.0-mm-diameter cylindrical probe. The probe was programmed to descend at a speed of 500 mm min^{-1} to a distance of 5 mm. Intact cucamelon fruit were positioned under the probe so that they were punctured approximately at the fruit equator. Flesh firmness was estimated as the peak force (N) measured during compression. Duplicate cucamelons from each wash treatment were tested on day of treatment and after 7, 14 and 21 of storage.

2.8 Colour measurement

Change to the colour of cucamelon skin on day of treatment and following 7, 14 and 21 days of storage was quantified using image analysis. Cucamelons were imaged with a Stereo microscope (SZM-45B2, Optex) and microscope camera (5 MP Microscope USB camera, Westlab). The stage was illuminated using a LED lighting panel (AL-F7, Aputure). Three photos covering random areas of each cucamelon were taken by gently rotating the fruit using sterile tweezers. Six cucamelons were photographed for each wash treatment and the experiment was repeated over three biological replicates performed on different days. To account for any changes in ambient lighting conditions, the cucamelons were photographed on the same white background. The colour values of the background of the photos in the linear RGB colour space were then standardised across all photos using R (R Core Team, 2020).

As the cucamelon surface is patterned with sections of light and dark green, these were analyzed separately using computer vision and statistical clustering methods. The sample images were firstly cropped to only contain the area of the melon itself. The 'superpixel' algorithm (35) was implemented as part of the OpenImageR package (36) which is a computer vision algorithm that determines groups of contiguous pixels based on their proximity and divides them into 300 sections. To classify each group identified by the superpixel algorithm as light or dark, the k-means clustering algorithm was applied on the median L*a*b* colour channel values. In this CIELab colour space system, the L-axis, a-plane, and b-plane detail the level of brightness, green/red and blue/yellow of a section, respectively.

For each sample, the average of each of the L*a*b* colour channels were identified individually for the light and dark sections. Total colour difference, Delta E (ΔE*) was calculated by the following equation where $_1$ and $_2$ indicate the values on day 0 and day 21.

$$\Delta E^*_{ab} = \sqrt{(L^*_2 - L^*_1)^2 + (a^*_2 - a^*_1)^2 + (b^*_2 - b^*_1)^2}$$

The browning index (BI) indicates the brown colour intensity of an image (37) calculated as:

$$\mathrm{BI} = 100\frac{\mathrm{x} - 0.31}{0.172};\ \mathrm{x} = \frac{(\mathrm{a}^* + 1.75\,\mathrm{L}^*)}{(5.645\,\mathrm{L}^* + \mathrm{a}^* - 3.012\,\mathrm{b}^*)}$$

The statistical significance of colour change between day 0 and day 21 was tested for both light and dark sections independently and for the two sections combined. Pairwise t-tests between each treatment group were performed using R. One-way ANOVA tests were also completed on the treatment type to see if treatment was a significant predictor of change between day 0 and day 21.

2.9 Sensory quality assessment

The effect of sanitizer treatments on the quality of cucamelons over 4 weeks of storage was assessed by 6 panellists using a sensory evaluation. The acceptability of the product was based on the freshness, appearance, deterioration and uniformity of the fruit. Panellists scored using a 5-point rating scale that described the fruit as: 1= extremely poor quality, inedible and with an unacceptable appearance; 2= poor quality, excessive defects and not useable; 3= low quality, moderately objectionable defects; 4= good quality with some minor defects; 5= excellent. Scores of 3 and lower indicated that the product was no longer within acceptable specifications for consumption. Panellists were blinded to sanitizer treatment, and six cucamelons were assessed from each treatment, with the experiment performed twice on different weeks.

2.10 Supporting plasma chemistry model and electric field analysis

To model the plasma chemistry and electric fields, the gas residence time, voltage, and current parameters of the DBDD system were first investigated. Based on the geometry of the reactor, the discharge volume was estimated to be 1 cm^3 and so the residence time of gas species within the discharge volume was calculated as 0.067 s at the gas flow rate of 1 SLM. The voltage and current characteristics of the DDBD reactor were measured using a

digital oscilloscope (DS61040, RIGOL) with a high voltage probe (PVM-6, North Star) and a current sensor (HET10AB15U10, PEMCH Tech.). The experimental configuration was as shown in Figure 1, including voltage and current measurement setup. The reduced electric field (E/N) is an important parameter for modelling and is defined by the ratio of E/N, where E is the electric field strength and N indicates the density of neutral gas molecules in the discharge. Due to the complexity and variability of the voltage-current measurements over time (Figure S1), multiple (E/N) values were chosen for the plasma chemistry simulation ranging from 30-50 Townsends (Td). The influence of these parameters on the production of $\cdot O_2^-$ and other important gas products listed in Table 2 was investigated.

A model of the plasma chemistry was then used to investigate the pathways of reactive species production in the DBDD system. Based on a previous N_2-H_2O plasma discharge model (38), a N_2/O_2 plasma chemistry model was developed that included more oxygen-related reactions to enable important gas products and predominant reaction pathways of $\cdot O_2^-$ to be investigated (Table S1). Open-source ZDPlaskin (39) combined with the Boltzmann equation solver BOLSIG+ (40, 41) were used to provide the reaction coefficients for different electron interactions, including electron attachment, ionization, vibrational and electronic excitation, dissociation, and important chemical reactions between N_2 and O_2, as listed in Tables S1 and S2. The gas phase chemical reactions between nitrogen and oxygen species were mostly adapted from a previous study (42). The gas phase reactions included in the kinetic input data were as presented in the reaction equation (1). These were converted into a coupled differential equation form of particle conservation equations (2) for individual species *i*, which included different production and loss reactions.

$$aA + bB \longrightarrow a'A + cC \quad (1)$$

$$\frac{d[N_i]}{dt} = \sum_{j=1}^{j_{max}} K_{ij}(t) \quad (2)$$

where, [*Ni*] is the density of species *i*, $K_A = (a' - a)k, K_B = -bk, Kc = ck, K_j = k_j[A]^a[B]^b$, k_j indicates the reaction coefficient of reaction (1).

Table 2. Gas phase considered in the N_2/O_2 plasma chemistry model

Ground-state molecules and radicals	N_2, O_2, O_3, NO, NO_2, NO_3, NO, NO_2, NO_3, N_2O, N_2O_3, N_2O_4, N_2O_5
Vibrationally excited molecules	$N_2(v_i, i=1\text{-}8)$, $O_2(v_i, i=1\text{-}4)$
Electronically excited molecules	$N_2(A3)$, $N_2(B3)$, $N_2(a`1)$, $N_2(C3)$, $O_2(a1)$ $O_2(b1)$
Atoms	N, N(2D), N(2P), O, O(1D), O(1S)
Ions	N^+, N_2^+, N_3^+, N_4^+, O^+, O_2^+, NO^+, N_2O^+, O^-, O_2^-

The Electrostatic Interface of COMSOL Multiphysics (V6.0) was used to simulate the spatial and temporal electric potential and field distribution with the peak voltage of 8 kV, 60 kHz AC applied at the high-voltage electrode as shown in Figure S1. A 2D axisymmetric model of the DBDD was taken to reduce the calculation time. The geometry of the reactor is shown in figure 2 (A). The dimensions were defined as a 2 mm diameter high-voltage (HV) electrode sheathed by a 1 mm thick glass tube, a 1 mm discharge gap and a 1 mm thick outer glass tube. The gas bubbles were defined by a 3 mm diameter filled with air. The cucamelon was simulated at two positions: at the bottom of the water as shown in Figure 2 (A), and at the top of the water as shown in Figure S3. The cucamelon was modelled as having 7 or 14 bacterial cells on its surface or floating in bulk water as shown in Figure 2 (B) and (C) and Figure S3. The bacteria were modelled with a long axis radius of 2 µm and a short axis radius 0.7 µm, presented in a simplified ellipse shape. The relative permittivity ($\varepsilon/\varepsilon_0$) of cucamelon skin was set as 3, as per a previous study (43) that assigned this value for apple skin. For the bacterial cell, a higher value of 15 was taken (44). The minimum and maximum size of the COMSOL mesh geometry was set as 0.1 µm and 0.5 mm to provide enough detail within the bacterial cell region as shown in Figure 2 (C). The normal component of the electric field (E) is calculated by ($\sqrt{E_r^2 + E_z^2}$), the normal polarization component (P) is calculated by ($\sqrt{P_r^2 + P_z^2}$) and the maximum current density (J) is calculated by ($\sqrt{J_r^2 + J_z^2}$) where the subscripts r and z indicate radial and axial components, respectively.

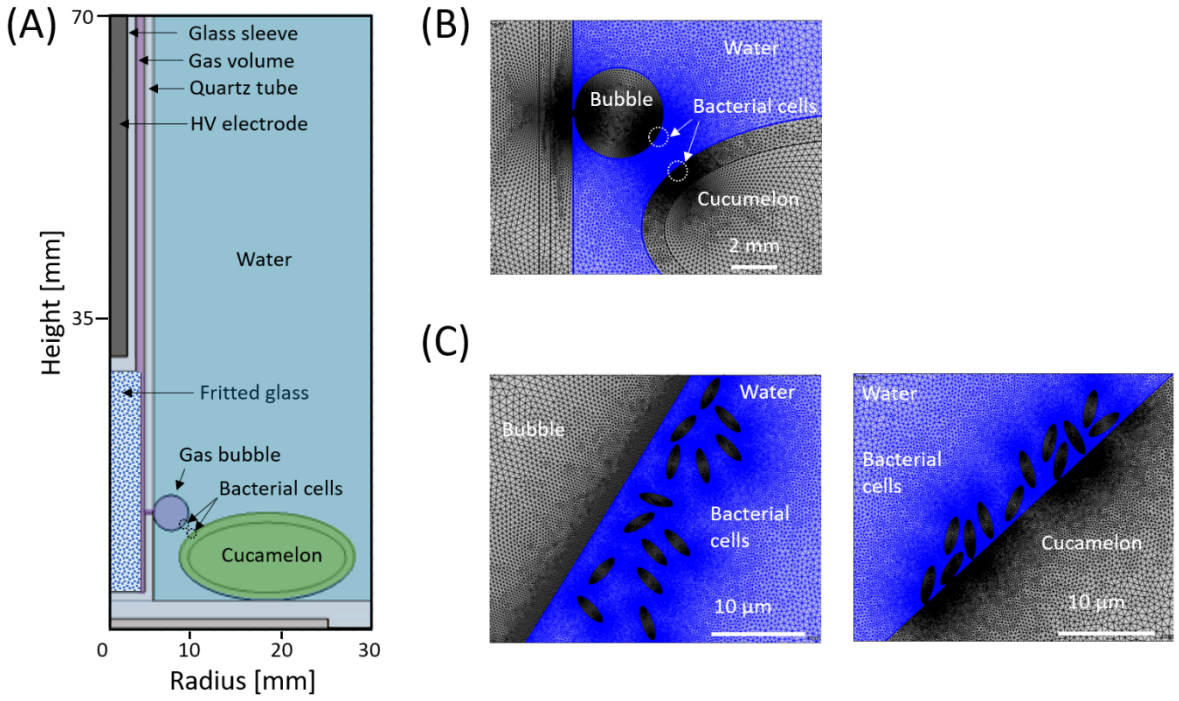

Figure 2. Schematic of the DBDD-PAW reactor containing the cucamelon and bacteria for electric field modelling with COMSOL. (A) DDBD reactor geometry including bacterial cells attached to the cucamelon skin for electric field analysis; (B) built-in mesh geometry for the COMSOL program near the bubble and cucamelon surface; (C) details of the modelled bacterial cells floating in solution close to the bubble (left) and on the cucamelon skin (right).

Results:

3.1 Reduction of pathogenic bacteria on the cucamelon surface and in wash water

The reduction of pathogens on the surfaces of cucamelons and in the wash water are shown in Figure 3. Two-minute treatments with PAW or NaOCl significantly reduced the counts of all pathogens on the cucamelon surface in comparison to the water control, with a 1 - 1.5 log CFU g^{-1} and 1.2 - 2.4 log CFU g^{-1} reduction in counts, respectively. In wash water, both sanitizers reduced 6 log CFU mL^{-1} of pathogenic bacteria to below detectible limits within the 2-minute treatment time. The addition of the $\cdot O_2^-$ scavenger tiron to DBDD-PAW treatment significantly increased survival of the pathogens in the wash water and on the cucamelon surface. This demonstrated that $\cdot O_2^-$ and/or reactive species produced by $\cdot O_2^-$ in solution are required for bacterial killing by DBDD-PAW.

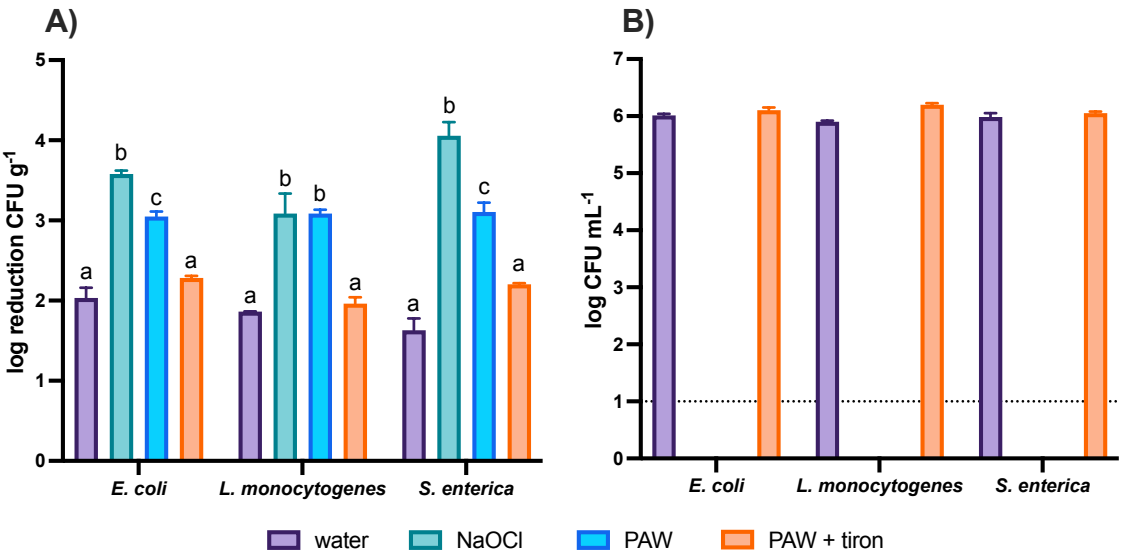

Figure 3. Survival of pathogenic bacteria in the wash water and adhered to the cucamelon surface following a 2-minute wash treatment. (A) Log reduction of bacterial CFU per gram on cucamelon surfaces compared to an unwashed control after 2-minute treatment with tap water, NaOCl (total chlorine 100 ppm and pH 6.5), PAW, or PAW with the $\cdot O_2^-$ scavenger tiron. (B) Survival of pathogenic bacteria in the wash solution after tap water, NaOCl, PAW or PAW and tiron treatments. *p* values of <0.05 are denoted by different letters. Error bars represent the standard error of the mean, and the dotted line denotes the limit of detection.

3.2 SEM of pathogenic bacteria on the cucamelon surface after sanitizer treatment

SEM was used to assess the impact of PAW and NaOCl treatment on the morphology of pathogenic microbes adhered to the surface of the cucamelons (Figure 4). The water-treated control cells were typically intact, smooth, and plump. Both NaOCl and PAW treatment led to distinct morphological changes. PAW treatment caused *E. coli* to have a deflated and ruptured cellular morphology, while *L. monocytogenes* cells had holes in the cell wall at the polar ends of the rods (white arrows, Figure 4). NaOCl treatment caused moderate crumpling or puckering of the cell surface in both species.

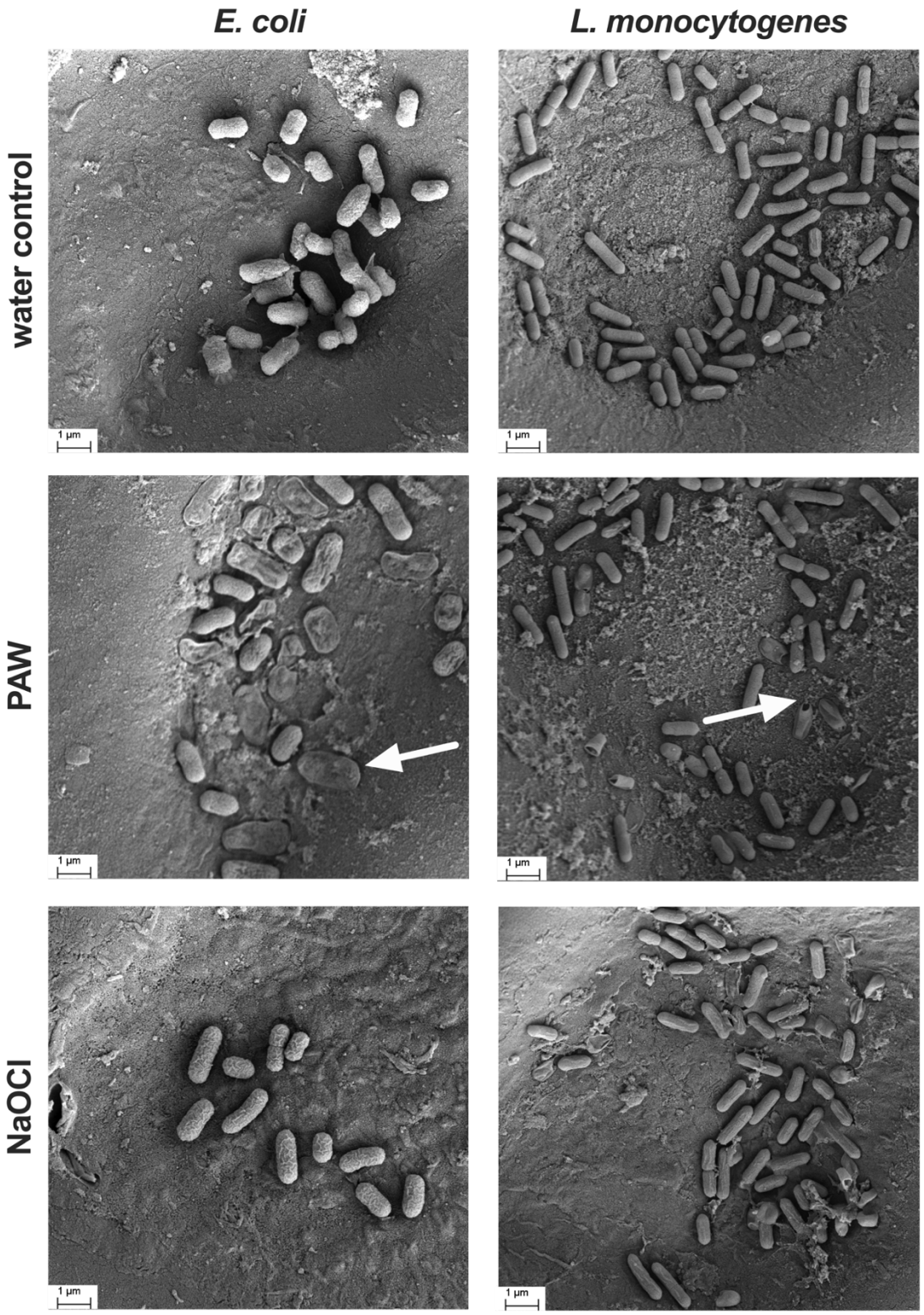

Figure 4. Scanning electron microscopy images of pathogenic bacteria adhered to the surface of cucamelons and treated with a 2-minute wash of water, PAW or NaOCl. Following PAW treatment, many of the *E. coli* cells exhibited a deflated, dehydrated, and crumpled cellular morphology (arrow on left panel), while some *L. monocytogenes* cells had a distinct rupturing from their outermost ends (arrow on right panel). The surface of the cells of both bacterial species were moderately crumpled following treated with NaOCl.

3.3 Quality and organoleptic properties of treated cucamelons over storage time

The effects of wash treatment on background microflora are shown in Figure 5 (A) and (B). Initial counts of total viable mesophilic bacteria counts (TVCs) on cucamelon surfaces were 5.9 log CFU g^{-1}, which were reduced by 0.8 log CFU g^{-1} following washing with tap water, 1.7 log CFU g^{-1} by PAW treatment, and 2.2 log CFU g^{-1} by NaOCl treatment. By the end of the storage trial, the TVCs were similar across the different treatments. Untreated cucamelons had 4.9 log CFU g^{-1} of background yeast and moulds that was not significantly reduced by treatment with water, while NaOCl and PAW treatment reduced counts by 1.5 log CFU g^{-1} and 2 log CFU g^{-1}, respectively. The background microflora that washed off the cucamelons and into the wash water was 3 log CFU mL^{-1} of TVCs and 2.6 log CFU mL^{-1} of yeast and mould. Treatment with PAW or NaOCl reduced these microbes in the wash water to below detectable limits.

Various quality parameters of the treated cucamelons were investigated. The firmness of the cucamelons directly after sanitizer treatment and over the 21 days of storage is shown in Figure 5 (C). Cucamelons that were treated with NaOCl were the softest of all the treatments from day 7 onwards, however, the only significant difference in texture in this series was that PAW-treated cucamelons were significantly firmer on the final day of the experiment compared to those treated with NaOCl. The colour metrics of light, dark and combined sections of cucamelons following different wash conditions were analyzed, with the total combined colour change over time for the light and dark sections shown in Figure 5 (D). The wash treatments did not result in significantly different colour changes between day of treatment and day 21 when compared using pairwise t-tests. On day 28, the sensory quality scores of NaOCl-treated cucamelons were on average below 3, and these cucamelons were of significantly poorer quality than those treated with PAW or water (Figure 5 E).

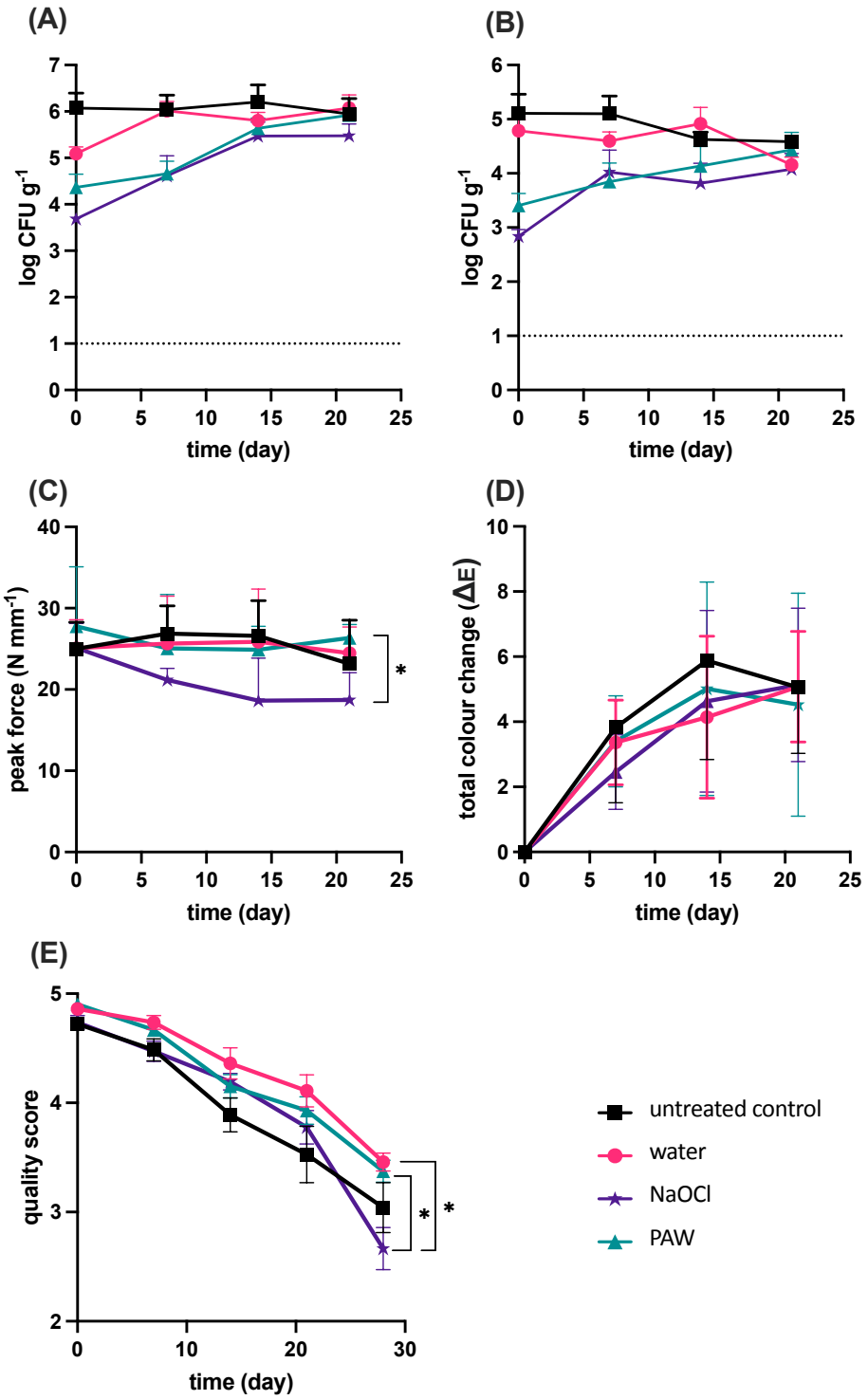

Figure 5. Quality parameters during storage of cucamelons following different wash treatments. (A) Counts of total viable mesophilic bacteria, (B) counts of total yeast and moulds, (C) texture of the cucamelons, with higher peak force units representing a firmer fruit, (D) total colour change of the surface of the cucamelons over time with the light and dark sections combined, (E) quality of cucamelons as scored by a panel marking organoleptic properties. *p* values of <0.05 are denoted by * and error bars represent standard error of the mean.

3.4 Plasma chemistry modelling to determine $\cdot O_2^-$ production

The electrical voltage and current characteristics of the DBDD plasma were determined in order to model the plasma chemistry and $\cdot O_2^-$ production of the system. The measured voltage, current response, and the calculated power from the DDBD reactor are shown in Figure S1. The peak voltage and current were 8 (±0.1) kV and 0.12 (±0.1) A, and the estimated average power dissipated to the plasma discharge was approximately 12 (± 0.24) W. The plasma discharge was complex and varied over time (Figure S1); therefore, a range of E/N values from 30 to 50 Td were simulated for the initial plasma chemistry modelling. Figure 6 (A) shows the kinetic modelling result with the predicted mole fraction of important gas species in the air discharge at these E/N conditions. At 30 Td, $\cdot O_2^-$ was predominant compared to the other reactive species in the air discharge. At the higher E/N values, the production of ozone and NOx species increased whereas $\cdot O_2^-$ production decreased. This was not reflective of the DBDD-PAW physicochemical properties defined by our previous analysis (29); therefore, 30 Td was the assumed E/N value used for subsequent modelling.

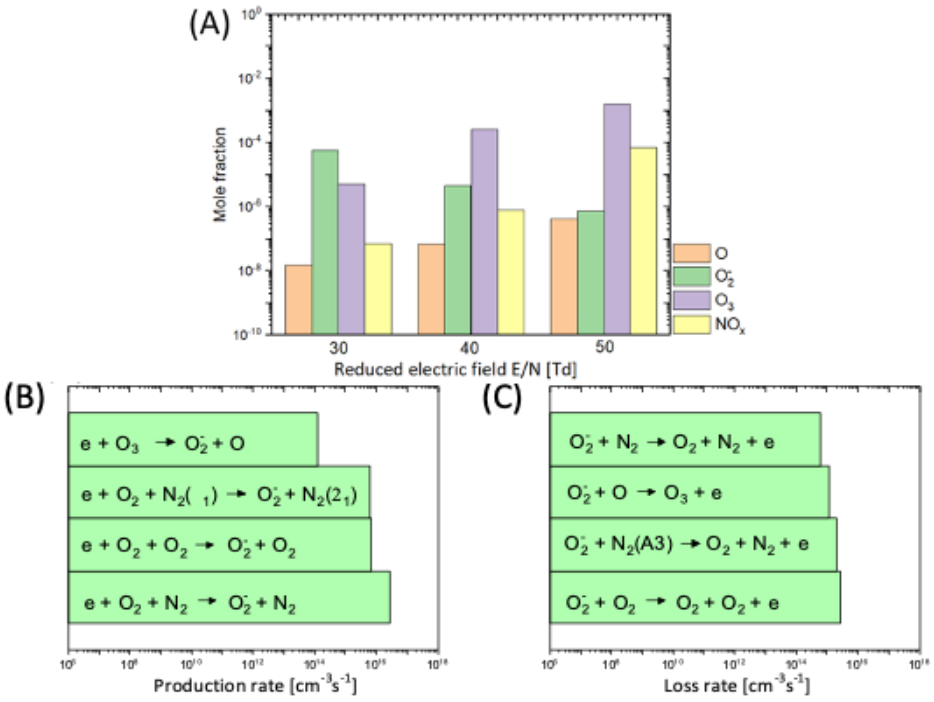

Figure 6. Plasma chemistry modelling of the N_2/O_2 plasma discharge at atmospheric pressure. (A) The mole fraction of important gas species produced by the DBDD plasma at E/N conditions of 30, 40 and 50 Td. NO_x indicates the sum of total NO species in the gas phase including NO, NO_2, NO_3, N_2O_3, N_2O_4 and N_2O_5. The important production (B) and loss (C) mechanisms and rates of O_2^- in the gas phase. The settings used for this modelling were glass transition temperature of 300K, residence time of 0.067s and a gas composition of N_2:O_2=0.8:0.2.

The plasma modelling results in Figure 6 (B) and (C) depict the production and loss mechanism of $\cdot O_2^-$ in the DBDD system. Three body attachment was the main pathway to generate $\cdot O_2^-$ in this model. This occurs when an electron attaches to the oxygen molecule to make $\cdot O_2^-$ and a third, neutral molecule such as N_2 or O_2 is present to absorb the released energy and complete the reaction.

$$e^- + O_2 + M \text{ (3rd body, any neutrals)} \Rightarrow \cdot O_2^- + M$$

In principle, this electron attachment process is most likely to occur at a low electron energy (<0.1 eV) due to the low threshold energy requirement as shown in Figure S2. However, a high electron density is required to increase the probability that this reaction will occur. The electron density is mainly determined by the E/N in a given reactor configuration. Therefore, operating in the optimum range of E/N and electron density is crucial for the effective production of $\cdot O_2^-$ with this DBDD system. At higher E/N conditions, there is a greater density of dissociated oxygen atoms and excited nitrogen molecules (Figure 6A) resulting in a high loss rate of $\cdot O_2^-$ (Figure 6C) and contributing to the competing production of O_3 or NO_x (Figure 6B). Taken together, these results show that lower E/N is required for efficient $\cdot O_2^-$ production.

3.5 Modelling of the electric field and its effect on bacterial cells

Figure 7 depicts the spatial distribution of the electric field and the polarization field in the DBDD reactor model at the peak applied voltage of 8 kV and 60 kHz AC input. As shown in Figure 7 (A), a strong electric field is formed in the discharge gap between glass sheath of the high voltage electrode, whereas in the rest of the dielectric domain, including the water and the cucamelon, the electric field is significantly attenuated. Figure 7 (B) shows the polarization field that is generated, which is particularly enhanced near the interface between the bubble and the cucamelon surface. A more detailed view of the local electric field and the positioning of the bacteria cells in relation to a plasma bubble and the cucamelon is shown in Figure 8 (A). Figure 8 (B) and (C) show the electric field distribution of bacterial cells floating in solution or attached to the cucamelon surface, respectively. These demonstrate that a high local electric field of over 2.0 kV/cm can be formed inside the bacterial cell under these conditions. This is strongly dependent on the relative position of individual bacterial cells; when the

cucamelon is located at the top of the water, the maximum local electric field experienced by the bacteria is much lower at 0.24 to 0.55 kV/cm (Figure S3). A highly enhanced local polarization field is observed at the tips of bacterial cells in solution (Figure 8 D) and between bacterial cells and the cucamelon skin (Figure 8 E). The largest induced polarization current density value was over 40 A/m^2 in this model. This modelling is reflected in the pattern of damage to PAW-treated *L. monocytogenes* cells seen in the SEM images (white arrow, Figure 4), indicating a possible influence of this strongly enhanced polarization current at the ends of the bacterial cells that leads to cell damage and ultimately cell death.

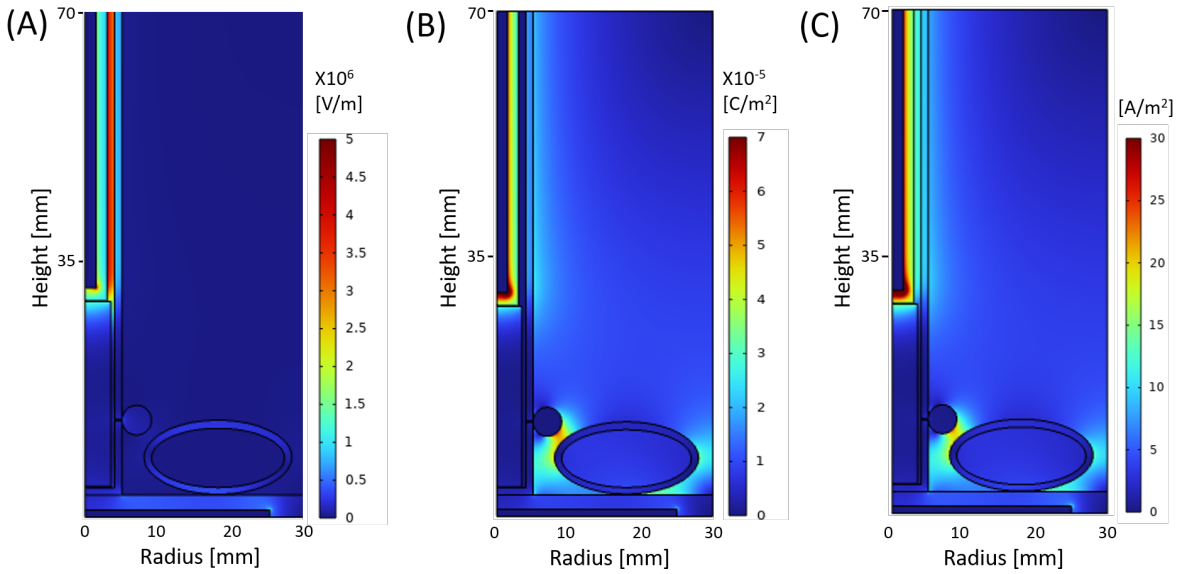

Figure 7. Modelling of the spatial distribution of the normal component of (A) electric field, (B) polarization and (C) maximum current density at the peak voltage 8 kV, in the entire configuration of the DDBD reactor.

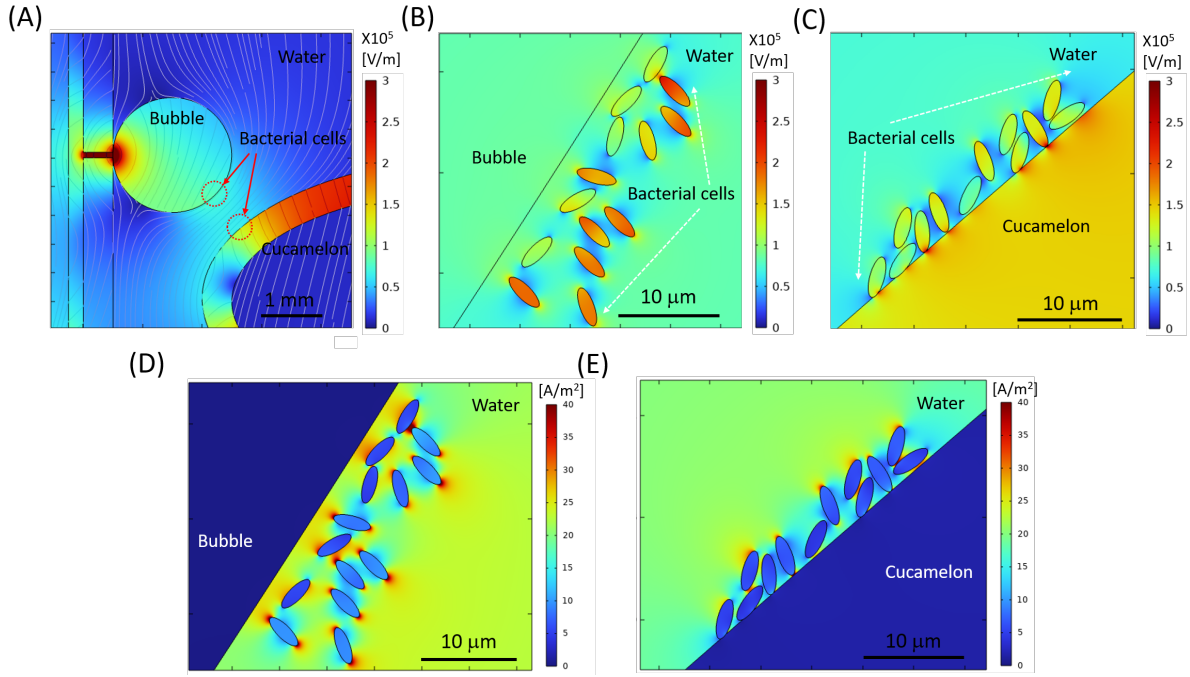

Figure 8. Modelling of the electric field distribution and charge accumulation for bacterial cells in the DBDD-PAW system. (A) Electric field analysis, where grey lines show the streamline of the electric field between the bubble and the cucamelon at peak voltage 8 kV. (B-C) Detailed local electric field distribution close to the bacterial cells shown next to the bubble (B), and on the cucamelon skin (C). (D-E) Simulated maximum current density distribution near bacterial cells floating in the water close to the bubble (D) and attached on the cucamelon skin (E).

Discussion

This study evaluated the sanitisation efficacy of an *in situ* PAW reactor in comparison to the established sanitizer NaOCl, using a cucurbit fresh produce model. We observed that treatment with PAW preserved the shelf life and quality of the cucamelons while effectively reducing microbial loads of the background flora as well as inoculated pathogenic bacteria. Although NaOCl was slightly more effective than PAW at reducing the counts of the pathogenic Gram-negative bacteria on the cucamelon surface, this sanitizer resulted in produce that was lower in quality over time. The mechanisms behind the acute antimicrobial power of the plasma system used in this study were explored, with $\cdot O_2^-$ shown to be an essential reactive species. Electric field and charge accumulation modelling demonstrated that bacteria on cucamelon surfaces and in the wash water experience strong electrical forces, which may act synergistically with the reactive species such as $\cdot O_2^-$ to produce powerful antibacterial activity.

There are growing calls to increase the consumption of fresh produce and to reduce food wastage, however this can be at odds with food safety requirements where strong sanitising agents may be needed to kill pathogens and reduce microbial load. In the current study, we used a cucamelon model in a small-scale DBDD plasma reactor and demonstrated that DBDD-PAW is a competitive sanitizer technology for fresh produce. A 2-minute treatment with either DBDD-PAW or NaOCl reduced 6 log CFU mL^{-1} bacterial pathogens in the wash water to below detectable limits. Furthermore, the *in situ* bubbling DBDD-PAW system used in the current study induced a substantially more rapid antimicrobial effect compared to previous PAW models, including a DBD electrode positioned above the water that required 40 minutes of treatment (45), or a remote DBD bubble system that required pre-activation of the water for more than 80 minutes (46), making this system more feasible for industrial use.

Bacteria that were adhered to the surface of the cucamelons were also significantly reduced by DBDD-PAW treatment. Pathogenic species *E. coli*, *S. enterica* and *L. monocytogenes* inoculated on the cucurbit surface were all reduced by 3 log CFU g^{-1} with DBDD-PAW compared to the unwashed control. A similar result has been reported using lettuce leaves and a bubbling DBD-PAW system, where a 2 log CFU g^{-1} reduction of *Listeria innocua* occurred after three minutes of treatment (26). NaOCl treatment was slightly more effective than PAW at reducing the gram-negative pathogens on the cucamelon surface, however, the two treatments were similarly effective in reducing *L. monocytogenes* populations. Longer pre-activation and treatment times may be required to optimise the antimicrobial power of PAW, however, this has challenges for steady-state operation and can reduce the quality of the fresh produce, as demonstrated in a recent study with kale and spinach (47). Overall, PAW treatment was highly effective at reducing the counts of pathogenic bacteria and demonstrated competitive antimicrobial efficacy to NaOCl treatment in a rapid 2-minute wash time.

Resident mesophilic fungi and bacteria are associated with postharvest spoilage of fresh produce (48), and these were rapidly reduced by the PAW treatment, giving similar results to treatment with NaOCl (Figure 5A and 5B). Comparable reductions have been reported for PAW treatment of baby spinach and rocket leaves, and for bean sprouts (49-51), indicating

application across a range of produce types. In addition, treatment with PAW maintained organoleptic quality and increased the shelf life of cucamelons over time in comparison to NaOCl. Enhanced textural quality following PAW has been demonstrated previously for button mushrooms (24), apples (52) and Chinese bayberries (53), and previous studies have reported that PAW treatment does not significantly alter the colour of grapes (22), lettuce (54) and spinach (50). In addition to effective sanitation, PAW treatment had no adverse effects on quality and resulted in fruit with superior texture and sensory evaluation scores than NaOCl treatment (Figure 5C and 5E). Together these findings indicate the capacity for DBDD-PAW treatment to both reduce pathogens and mesophiles, while extending shelf life and maintaining a high quality of the produce, indicating better performance overall in comparison to the established sanitizer, NaOCl.

Modelling suggested PAW treatment caused a highly localized surface charge density on the poles of the bacterial cells, which was supported by the SEM analysis showing the PAW-treated bacteria ruptured at their ends. This dramatic physical disruption is very similar to the appearance of cells following pulsed electric field treatment (55) and was quite distinct from NaOCl treatment, where crumpling and puckering of the cell surface was observed. At and near the interface of different materials such as water/bacterial cell or bacterial cell/cucamelon skin, a high-density surface charge can be generated by the dipole-like response of dielectric material, and this leads to a strong local polarization and electric field. The induced current density at the interface of bacterial cells and water was found to reach a very high value of over 4.0 mA/cm^2. Membrane damage and leakage of bacterial cells has been observed in a much lower current range of 50 – 80 μA/cm^2, although this was after a longer treatment time of 30 minutes and with direct current conditions (56). Regardless, charges of opposite polarity in membranes oscillate according to the applied electric field, leading to a strong polarization field and induced currents. We hypothesize that this physical effect may have caused the observed membrane stresses and pore formation, especially where the highly localized surface charge density was accumulating at the ends of the rod-shaped cells.

The superoxide anion ($\cdot O_2^-$) has previously been demonstrated to be critical for the antimicrobial activity of the DBDD-PAW (29), and this was confirmed in the current study

where the addition of tiron, a $\cdot O_2^-$ scavenger, significantly reduced the antimicrobial activity of the DBDD-PAW. $\cdot O_2^-$ has a short half-life and a negative charge when in a solution with a neutral pH (57) which would typically prevent it from passing through the membrane of bacterial cells (58). Therefore, while $\cdot O_2^-$ is required for antimicrobial power, this reactive species on its own may not be sufficient for the activity observed. Previous studies have demonstrated that the $\cdot O_2^-$ produced in a DBD-PAW is a precursor to highly antimicrobial reactive species such as hydroxyl radicals and singlet molecular oxygen, and these secondary reactive species have been shown to contribute to the potent antimicrobial effects of PAW on yeast (59) and *Salmonella* Typhimurium (60). Therefore, $\cdot O_2^-$ and/or downstream reactive species, combined with the physical effects of the *in situ* plasma treatment that result in membrane damage and permeabilization, are likely synergising to create the powerful antimicrobial effects produced by DBDD-PAW.

PAW technologies that rely on $\cdot O_2^-$ may be more cost effective and more readily applied to industrial applications than those relying on other reactive oxygen and nitrogen species (RONS) for the *in situ* treatment of fresh produce. As an ionic species, $\cdot O_2^-$ can dissolve directly into water without loss, unlike other RONS species such as NO or O_3 that have a low solubility in water (61). This rapid solvation of $\cdot O_2^-$ means pre-activation or long treatment times are not required for DBDD-PAW, unlike PAW systems where less soluble RONS provide the antimicrobial power (29). In addition, the formation and accumulation of $\cdot O_2^-$ occurs at a lower electron energy and E/N compared to other RONS (Figure S2) (62) and the power requirements of the DBDD are very low at only 12 W (Figure S1) . Finally, the DBDD-PAW system does not increase the temperature of the water substantially or produce large concentrations of longer-lived reactive species such as nitrates and nitrites that have been seen with a spark discharge PAW reactor (29), so there are no requirements for cooling systems and fewer concerns with chemical residues on the fresh produce.

The findings presented in this study indicate that the DBDD-PAW system is a competitive sanitizer technology that warrants upscaling for postharvest treatment of fresh produce. This system may be advantageous over traditional chemical sanitizers in terms of sustainability and cost as powerful antimicrobial power is achieved with only air, tap water, the plasma reactor and low amounts of electricity (12 W), and there is no need to dispose of

hazardous effluents. PAW treatment extended the quality of the fresh produce to a greater extent than NaOCl, and the DBDD-PAW system used here reduced pathogenic bacteria more rapidly and without the often required pre-activation step by other PAW systems (45, 46). However, the activity of DBDD-PAW relies on the short-lived reactive species $\cdot O_2^-$ and the effects of an electric field and will be most effective when applied in an *in-situ* wash system. For future scale-up of this technology, reactor design and positioning in the wash systems must be considered to guarantee effective antimicrobial power and thereby maximize food safety.

Acknowledgements

The authors acknowledge the technical and scientific assistance of Sydney Microscopy & Microanalysis, the University of Sydney node of Microscopy Australia. The authors would also like to acknowledge associate professor Nicholas Coleman for generously growing the cucamelons for this study.

Funding

This research was conducted within the Australian Research Council Industrial Transformation Training Centre for Food Safety in the Fresh Produce Industry (Grant number: IC160100025) funded by the Australian Research Council, industry partners from Australia and New Zealand and administered by the University of Sydney.

Conflicts of interest

PJ Cullen is the CTO of Plasmaleap Technologies, the supplier of the plasma technology employed to generate plasma bubbles in this study.

References

1. Olaimat AN, Holley RA. 2012. Factors influencing the microbial safety of fresh produce: A review. Food Microbiology 32:1-19.
2. S. Paramithiotis EHD, P.N. Skandamis. Microbial ecology of fruits and fruit-based products, p 358-381, Quantitative Microbiology in Food Processing doi:10.1002/9781118823071.ch18.
3. Zheng J, Kase, J. , De Jesus, A. , Sahu, S. , Hayford, A. , Luo, Y. , Datta, A. , Brown, E. and Bell, R. Microbial ecology of fresh vegetables, p 339-357, Quantitative Microbiology in Food Processing doi:10.1002/9781118823071.ch17.
4. Gagliardi JV, Millner PD, Lester G, Ingram D. 2003. On-farm and postharvest processing sources of bacterial contamination to melon rinds. Journal of Food Protection 66:82-87.
5. Premier R. 2012. Evaluation of vegetable washing chemicals Global F.S. Pty Ltd, Ltd HA, Sydney.
6. Gombas D, Luo Y, Brennan J, Shergill G, Petran R, Walsh R, Hau H, Khurana K, Zomorodi B, Rosen J, Varley R, Deng K. 2017. Guidelines To Validate Control of

Cross-Contamination during Washing of Fresh-Cut Leafy Vegetables. Journal of Food Protection 80:312-330.

7. Sapers GM. 2001. Efficacy of washing and sanitizing methods for disinfection of fresh fruit and vegetable products. Food Technology and Biotechnology 39:305-311.
8. Murray K, Wu F, Shi J, Xue SJ, Warriner K. 2017. Challenges in the microbiological food safety of fresh produce: Limitations of post-harvest washing and the need for alternative interventions. Food Quality and Safety 1:289-301.
9. Luo YG, Nou XW, Yang Y, Alegre I, Turner E, Feng H, Abadias M, Conway W. 2011. Determination of Free Chlorine Concentrations Needed To Prevent Escherichia coli O157:H7 Cross-Contamination during Fresh-Cut Produce Wash. Journal of Food Protection 74:352-358.
10. Luo YG, Nou XW, Millner P, Zhou B, Shen CL, Yang Y, Wu YP, Wang Q, Feng H, Shelton D. 2012. A pilot plant scale evaluation of a new process aid for enhancing chlorine efficacy against pathogen survival and cross-contamination during produce wash. International Journal of Food Microbiology 158:133-139.
11. Hua GH, Reckhow DA. 2007. Comparison of disinfection byproduct formation from chlorine and alternative disinfectants. Water Research 41:1667-1678.
12. Hung YC, Waters BW, Yemmireddy VK, Huang CH. 2017. pH effect on the formation of THM and HAA disinfection byproducts and potential control strategies for food processing. Journal of Integrative Agriculture 16:2914-2923.
13. Teng Z, Luo YG, Alborzi S, Zhou B, Chen L, Zhang JL, Zhang BC, Millner P, Wang Q. 2018. Investigation on chlorine-based sanitization under stabilized conditions in the presence of organic load. International Journal of Food Microbiology 266:150-157.
14. Huang AT, Batterman S. 2010. Sorption of trihalomethanes in foods. Environment International 36:754-762.
15. Gil MI, Marin A, Andujar S, Allende A. 2016. Should chlorate residues be of concern in fresh-cut salads? Food Control 60:416-421.
16. Grellier J, Rushton L, Briggs DJ, Nieuwenhuijsen MJ. 2015. Assessing the human health impacts of exposure to disinfection by-products - A critical review of concepts and methods. Environment International 78:61-81.
17. Olmez H, Kretzschmar U. 2009. Potential alternative disinfection methods for organic fresh-cut industry for minimizing water consumption and environmental impact. Lwt-Food Science and Technology 42:686-693.
18. Cullen PJ, Lalor J, Scally L, Boehm D, Milosavljević V, Bourke P, Keener K. 2018. Translation of plasma technology from the lab to the food industry. Plasma Processes and Polymers 15.
19. Zhou RW, Zhou RS, Wang PY, Xian YB, Mai-Prochnow A, Lu XP, Cullen PJ, Ostrikov K, Bazaka K. 2020. Plasma-activated water: generation, origin of reactive species and biological applications. Journal of Physics D-Applied Physics 53:27.
20. Ma RN, Wang GM, Tian Y, Wang KL, Zhang JE, Fang J. 2015. Non-thermal plasma-activated water inactivation of food-borne pathogen on fresh produce. Journal of Hazardous Materials 300:643-651.
21. Gan Z, Zhang Y, Gao W, Wang S, Liu Y, Xiao Y, Zhuang X, Sun A, Wang R. 2022. Effects of nonthermal plasma-activated water on the microbial sterilization and storage quality of blueberry. Food Bioscience 49.
22. Guo J, Huang K, Wang X, Lyu C, Yang N, Li Y, Wang J. 2017. Inactivation of yeast on grapes by plasma-activated water and its effects on quality attributes. Journal of Food Protection 80:225-230.

23. Joshi I, Salvi D, Schaffner DW, Karwe MV. 2018. Characterization of microbial inactivation using plasma-activated water and plasma-activated acidified buffer. Journal of Food Protection 81:1472-1480.
24. Xu YY, Tian Y, Ma RN, Liu QH, Zhang J. 2016. Effect of plasma activated water on the postharvest quality of button mushrooms, Agaricus bisporus. Food Chemistry 197:436-444.
25. Frohling A, Ehlbeck J, Schluter O. 2018. Impact of a Pilot-Scale Plasma-Assisted Washing Process on the Culturable Microbial Community Dynamics Related to Fresh-Cut Endive Lettuce. Applied Sciences-Basel 8.
26. Patange A, Lu P, Boehm D, Cullen PJ, Bourke P. 2019. Efficacy of cold plasma functionalised water for improving microbiological safety of fresh produce and wash water recycling. Food Microbiology 84.
27. Simon S, Salgado B, Hasan MI, Sivertsvik M, Fernández EN, Walsh JL. 2022. Influence of Potable Water Origin on the Physicochemical and Antimicrobial Properties of Plasma Activated Water. Plasma Chemistry and Plasma Processing 42:377-393.
28. Herianto S, Hou C-Y, Lin C-M, Chen H-L. 2021. Nonthermal plasma-activated water: A comprehensive review of this new tool for enhanced food safety and quality. Comprehensive Reviews in Food Science and Food Safety 20:583-626.
29. Rothwell JG, Alam D, Carter DA, Soltani B, McConchie R, Zhou RW, Cullen PJ, Mai-Prochnow A. 2022. The antimicrobial efficacy of plasma-activated water against Listeria and E. coli is modulated by reactor design and water composition. Journal of Applied Microbiology 132:2490-2500.
30. Herianto S, Hou CY, Lin CM, Chen HL. 2021. Nonthermal plasma-activated water: A comprehensive review of this new tool for enhanced food safety and quality. Compr Rev Food Sci Food Saf 20:583-626.
31. Mentheour R, Machala Z. 2022. Coupled Antibacterial Effects of Plasma-Activated Water and Pulsed Electric Field. Frontiers in Physics 10.
32. Reina LD, Fleming HP, Breidt Jr F. 2002. Bacterial contamination of cucumber fruit through adhesion. Journal of Food Protection 65:1881-1887.
33. Guo L, Xu RB, Gou L, Liu ZC, Zhao YM, Liu DX, Zhang L, Chen HL, Kong MG. 2018. Mechanism of Virus Inactivation by Cold Atmospheric-Pressure Plasma and Plasma-Activated Water. Applied and Environmental Microbiology 84:10.
34. (ed). 2016. Postharvest management of vegetables: Australian supply chain handbook. Horticulture Innovation Australia Limited, Accessed
35. Achanta R, Shaji A, Smith K, Lucchi A, Fua P, Süsstrunk S. 2012. SLIC Superpixels Compared to State-of-the-Art Superpixel Methods. IEEE Transactions on Pattern Analysis and Machine Intelligence 34:2274-2282.
36. Mouselimis L. 2022. OpenImageR: An Image Processing Toolkit, v R package version 1.2.5. https://CRAN.R-project.org/package=OpenImageR.
37. Buera MdP, Lozano R, Petriella C. 1986. Definition of colour in the non enzymatic browning process. Die Farbe 32:318-322.
38. Hong JM, Zhang TQ, Zhou RW, Dou LG, Zhang S, Zhou RS, Ashford B, Shao T, Murphy AB, Ostrikov K, Cullen PJ. 2022. Green chemical pathway of plasma synthesis of ammonia from nitrogen and water: a comparative kinetic study with a N-2/H-2 system. Green Chemistry 24:7458-7468.
39. Pancheshnyi S, Eismann B, Hagelaar GJM, Pitchford LC. 2008 Computer code ZDPlasKin (Toulouse: University of Toulouse, LAPLACE, CNRS-UPS-INP) (wwwzdplaskinlaplaceuniv-tlsefr).

40. Hagelaar GJM, Pitchford LC. 2005. Solving the Boltzmann equation to obtain electron transport coefficients and rate coefficients for fluid models. Plasma Sources Science and Technology 14:722-733.
41. BOLSIG+. Computer code doi:http://www.bolsig.laplace.univ-tlse.fr/.
42. Capitelli M, Ferreira CM, Gordiets BF, Osipov AI. 2000. Plasma Kinetics in Atmospheric Gases. Plasma Physics and Controlled Fusion 43:371-372.
43. Cheng H, Liu X, Lu X, Liu D. 2016. Active species delivered by dielectric barrier discharge filaments to bacteria biofilms on the surface of apple. Physics of Plasmas 23:073517.
44. Maurício R, Dias CJ, Santana F. 2006. Monitoring biofilm thickness using a non-destructive, on-line, electrical capacitance technique. Environ Monit Assess 119:599-607.
45. Berardinelli A, Pasquali F, Cevoli C, Trevisani M, Ragni L, Mancusi R, Manfreda G. 2016. Sanitisation of fresh-cut celery and radicchio by gas plasma treatments in water medium. Postharvest Biology and Technology 111:297-304.
46. Jyung S, Kang J-W, Kang D-H. 2022. L. monocytogens exhibited less cell membrane damage, lipid peroxidation, and intracellular reactive oxygen species accumulation after plasma-activated water treatment compared to E. coli O157:H7 and S. Typhimurium. Food Microbiology 108:104098.
47. Perinban S, Orsat V, Lyew D, Raghavan V. 2022. Effect of plasma activated water on Escherichia coli disinfection and quality of kale and spinach. Food Chemistry 397:133793.
48. Tournas VH. 2005. Spoilage of vegetable crops by bacteria and fungi and related health hazards. Crit Rev Microbiol 31:33-44.
49. Laurita R, Gozzi G, Tappi S, Capelli F, Bisag A, Laghi G, Gherardi M, Cellini B, Abouelenein D, Vittori S, Colombo V, Rocculi P, Dalla Rosa M, Vannini L. 2021. Effect of plasma activated water (PAW) on rocket leaves decontamination and nutritional value. Innovative Food Science & Emerging Technologies 73:102805.
50. Risa Vaka M, Sone I, García Álvarez R, Walsh JL, Prabhu L, Sivertsvik M, Noriega Fernández E. 2019. Towards the Next-Generation Disinfectant: Composition, Storability and Preservation Potential of Plasma Activated Water on Baby Spinach Leaves. Foods (Basel, Switzerland) 8:692.
51. Xiang Q, Liu X, Liu S, Ma Y, Xu C, Bai Y. 2019. Effect of plasma-activated water on microbial quality and physicochemical characteristics of mung bean sprouts. Innovative Food Science & Emerging Technologies 52:49-56.
52. Liu C, Chen C, Jiang A, Sun X, Guan Q, Hu W. 2020. Effects of plasma-activated water on microbial growth and storage quality of fresh-cut apple. Innovative Food Science & Emerging Technologies 59:102256.
53. Ma R, Yu S, Tian Y, Wang K, Sun C, Li X, Zhang J, Chen K, Fang J. 2016. Effect of Non-Thermal Plasma-Activated Water on Fruit Decay and Quality in Postharvest Chinese Bayberries. Food and Bioprocess Technology 9:1825-1834.
54. Schnabel U, Andrasch M, Stachowiak J, Weit C, Weihe T, Schmidt C, Muranyi P, Schlüter O, Ehlbeck J. 2019. Sanitation of fresh-cut endive lettuce by plasma processed tap water (PPtW) – Up-scaling to industrial level. Innovative Food Science & Emerging Technologies 53:45-55.
55. Estifaee P, Su X, Yannam SK, Rogers S, Thagard SM. 2019. Mechanism of E. coli Inactivation by Direct-in-liquid Electrical Discharge Plasma in Low Conductivity Solutions. Sci Rep 9:2326.

56. Krishnamurthi VR, Rogers A, Peifer J, Niyonshuti, II, Chen J, Wang Y. 2020. Microampere Electric Current Causes Bacterial Membrane Damage and Two-Way Leakage in a Short Period of Time. Appl Environ Microbiol 86.
57. Phaniendra A, Jestadi DB, Periyasamy L. 2015. Free Radicals: Properties, Sources, Targets, and Their Implication in Various Diseases. Indian Journal of Clinical Biochemistry 30:11-26.
58. Korshunov SS, Imlay JA. 2002. A potential role for periplasmic superoxide dismutase in blocking the penetration of external superoxide into the cytosol of Gram-negative bacteria. Molecular Microbiology 43:95-106.
59. Xu HB, Zhu YP, Du MR, Wang YQ, Ju SY, Ma RN, Jiao Z. 2021. Subcellular mechanism of microbial inactivation during water disinfection by cold atmospheric-pressure plasma. Water Research 188:16.
60. Baek KH, Heo YS, Park JY, Kang T, Lee YE, Lim J, Kim SB, Jo C. 2020. Inactivation of Salmonella Typhimurium by Non-Thermal Plasma Bubbles: Exploring the Key Reactive Species and the Influence of Organic Matter. Foods 9.
61. Lietz AM, Kushner MJ. 2016. Air plasma treatment of liquid covered tissue: long timescale chemistry. Journal of Physics D: Applied Physics 49:425204.
62. Wang W, Patil B, Heijkers S, Hessel V, Bogaerts A. 2017. Nitrogen Fixation by Gliding Arc Plasma: Better Insight by Chemical Kinetics Modelling. ChemSusChem 10:2145-2157.
63. M. Capitelli CF, B. Gordiets and A. Osipov. 2000. Plasma Kinetics in Atmospheric Gases doi:10.1088/0741-3335/43/3/702. Springer-Verlag Berlin.
64. Kossyi I, Kostinskiy A, Matveyev A, Silakov V. 1992. Kinetic scheme of the non-equilibrium discharge in nitrogen-oxygen mixtures. Plasma Sources Sci Technol 1:207-220.
65. Itikawa Y, Mason N. 2005. Cross Sections for Electron Collisions with Water Molecules J Phys Chem Ref Data 34:1.
66. Stafford DS, Kushner MJ. 2004. O2(Δ1) production in He⁄O2 mixtures in flowing low pressure plasmas. Journal of Applied Physics 96:2451-2465.
67. Gordiets BF, Ferreira CM, Guerra VL, Loureiro JMAH, Nahorny J, Pagnon D, Touzeau M, Vialle M. 1995. Kinetic model of a low-pressure N/sub 2/-O/sub 2/ flowing glow discharge. IEEE Transactions on Plasma Science 23:750-768.

Supporting information

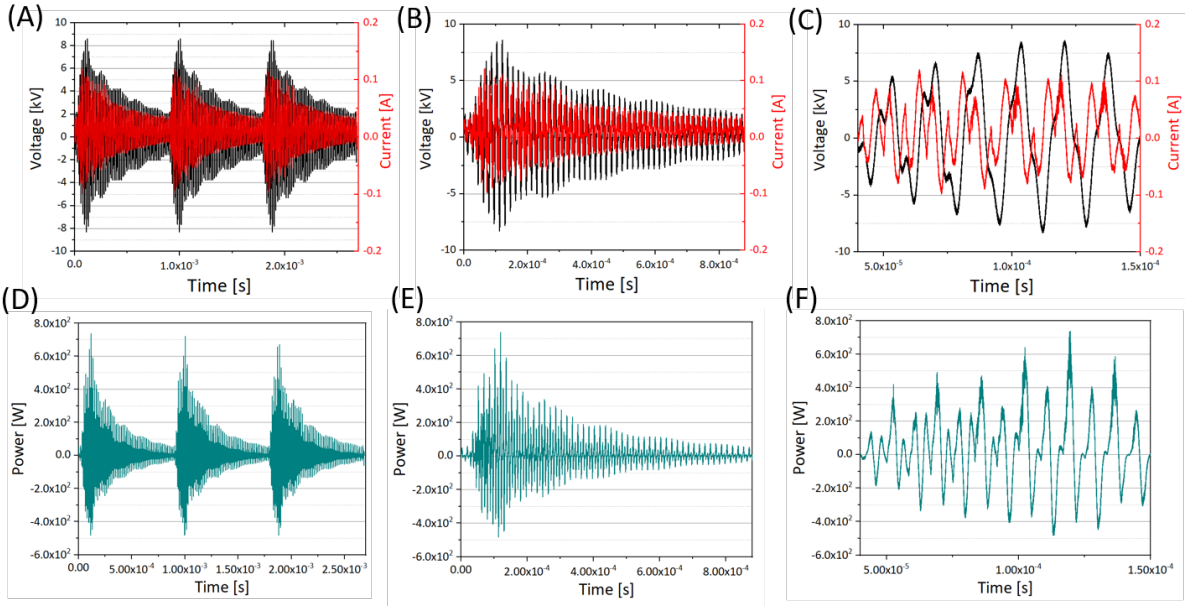

Figure S1. The electric waveforms of the measured voltage and current characteristics of the DBDD plasma (A)-(C) and the calculated output power of the DBDD plasma over different time scales (D)-(F).

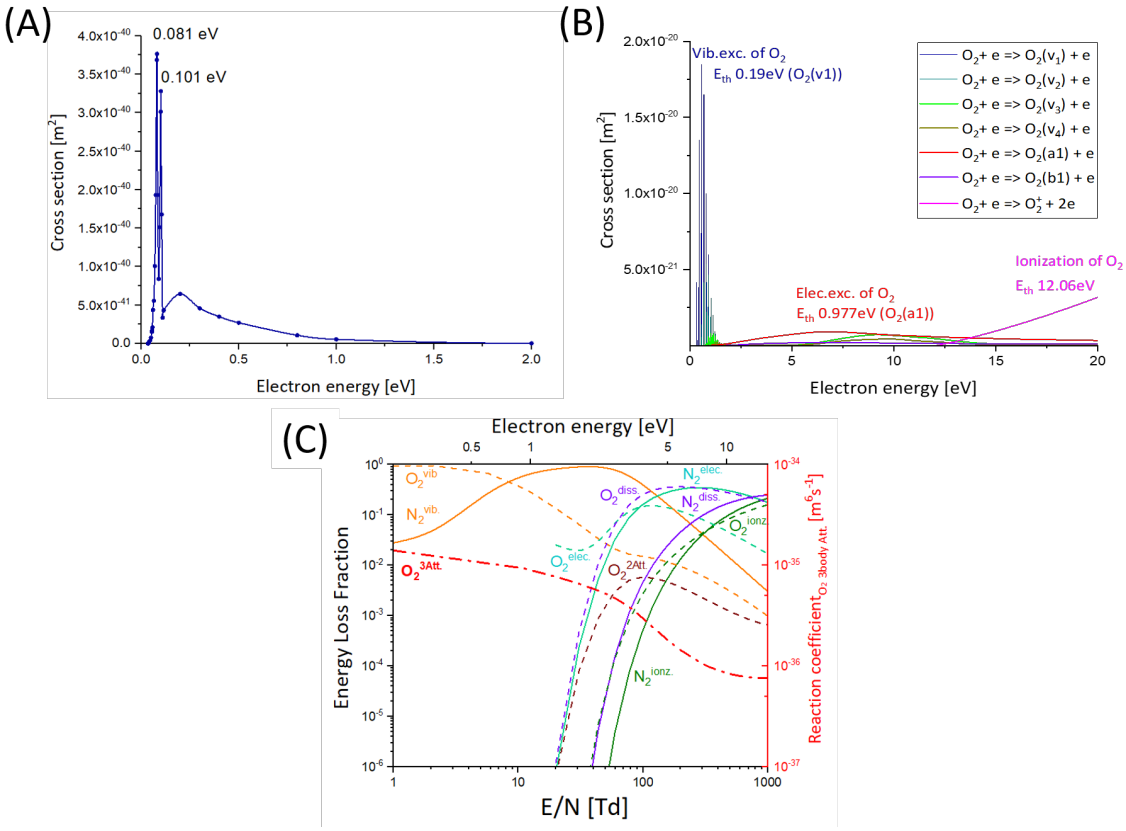

Figure S2. The reaction probability and energy loss fractions of electron interactions in the air plasma. The cross section data of (A) the 3 body electron attachment to produce O_2^-, and (B) other excitation and ionization reactions of oxygen as a function of electron energy, where Vib.exc. and Elec.exc. indicate vibrational excitation and electronic excitation, respectively. The energy loss fraction for different electron interactions in air plasma (C), where the gas composition of N_2:O_2=0.8:0.2, 1atm at 300 K. Due to the different physical dimensions of energy loss coefficient of 3 body process [eVm^6s^{-1}] in comparison to 2 body process[eVm^3s^{-1}],

this is presented in reaction coefficient [m^6s^{-1}] to show the reduced electric field E/N and electron energy dependence.

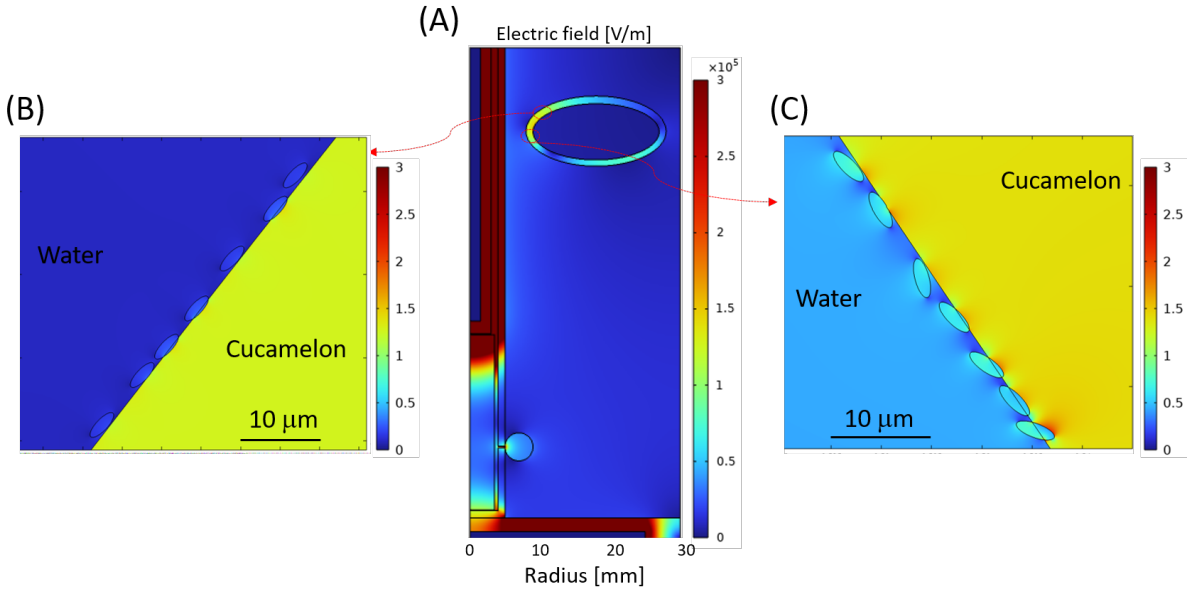

Figure S3. Modelling of the electric field distribution for bacterial cells when the cucamelon is positioned towards the top of the water in the DBDD-PAW system. (A) Modelling of the spatial distribution of the normal component of the electric field in the DBDD-PAW system at the peak voltage of 8 kV. The local electric field distribution surrounding the bacterial cells when next to the plasma bubble (A) or when adhered to the cucamelon surface (B).

Table S1. Summarized important gas phase reactions in N_2/O_2 plasma system; the gas temperature T_g and electron temperature T_e are in the unit of Kelvin [K]. M indicates any neutral if there is not given any specification.

	Process	Rate coefficient [cm^3s^{-1}] [cm^6s^{-1}] ǂ	Ref.
Reactions related to atomic oxygen			
R1	$O + NO + N_2 \rightarrow NO_2 + N_2$	$1.2\times10^{-31}(300/T_{gas})^{1.8}$	(63)
R2	$O + NO + NO \rightarrow NO_2 + NO$	$0.78\times1.2\times10^{-31}(300/T_{gas})^{1.8}$	(63)
R3	$O + NO + O_2 \rightarrow NO_2 + O_2$	$0.78\times1.2\times10^{-31}(300/T_{gas})^{1.8}$	(63)
R4	$O + NO_2 + N_2 \rightarrow NO_3 + N_2$	$8.9\times10^{-32}(300/T_{gas})^{2}$	(63)
R5	$O + NO_2 + NO \rightarrow NO_3 + NO$	$2.4\times8.9\times10^{-32}(300/T_{gas})^{2}$	(63)
R6	$O + NO_2 + O_2 \rightarrow NO_3 + O_2$	$8.9\times10^{-32}(300/T_{gas})^{2}$	(63)
R7	$O + NO \rightarrow NO_2 + \gamma$	4.2×10^{-18}, γ indicates photon emission	(63)
R8	$O + NO_2 \rightarrow NO + O_2$	$9.1\times10^{-12}(T_{gas}/300)^{0.18}$	(63)
R9	$O + NO_3 \rightarrow O_2 + NO_2$	1×10^{-11}	(63)
R10	$O + M \rightarrow NO + N$	Equation S1§ for M = $N_2(X)$, $N_2(v_i)$	(63)
R11	$O + N_2(A3) \rightarrow NO + N(2D)$	7.8×10^{-12}	(64)
R12	$O + N_2 + M \rightarrow N_2O + M$	$3.9\times10^{-35}\exp(-10400/T_{gas})$	(63)
R12	$O + N_2O \rightarrow NO + NO$	$1.5\times10^{-10}\exp(-14090/T_{gas})$	(63)
R13	$O + N + M \rightarrow NO + M$	$1.8\times10^{-31}(300/T_{gas})$, M = N, O, NO	(63)

		$1\times10^{-32}(300/T_{gas})^{0.5}$ for the rest neutrals	
R14	$O + O + N_2 \rightarrow O_2 + N_2$	$2.8\times10^{-34}\exp(720/T_{gas})$	(63)
R15	$O + O + O_2 \rightarrow O_2 + O_2$	$4.0\times10^{-33}(300/T_{gas})^{0.41}$	(63)
R16	$O + O + O \rightarrow O_2 + O$	$3.6\times4.0\times10^{-33}(300/T_{gas})^{0.41}$	(63)
R17	$O + O + N \rightarrow O_2 + N$	$0.8\times4.0\times10^{-33}(300/T_{gas})^{0.41}$	(63)
R18	$O + O + NO \rightarrow O_2 + NO$	$0.17\times4.0\times10^{-33}(300/T_{gas})^{0.41}$	(63)
R19	$O + O_2 + M \rightarrow O_3 + M$	$7.6\times10^{-34}(300/T_{gas})^{1.9}$, M = O_2, NO, NO_2, NO_3	(63)
		$3.9\times10^{-33}*(300/T_{gas})^{1.9}$, M = N, O	(63)
		$5.8\times10^{-34}*(300/T_{gas})^{2.8}$ for the rest neutrals	
R20	$O + O_2^- \rightarrow O_3 + e$	1.5×10^{-10}	(63)
R21	$O + O^- \rightarrow O_2 + e$	5.0×10^{-10}	(65, 66)
Interactions with atomic nitrogen			
R22	$N + O^- \rightarrow NO + e$	2.6×10^{-10}	(63)
R23	$N + O_2^- \rightarrow NO_2 + e$	5.0×10^{-10}	(63)
R24	$N + NO \rightarrow O + N_2$	$1.8\times10^{-11}(T_{gas}/300)^{0.5}$	(63)
R25	$N + O_2 \rightarrow O + NO$	$3.2\times10^{-12}(T_{gas}/300)\exp(-3150/T_{gas})$	(63)
R26	$N + O_2(a1) \rightarrow O + NO$	$2\times10^{-14}\exp(-600/T_{gas})$	(67)
R27	$N + NO_2 \rightarrow 2O + N_2$	9.1×10^{-13}	(63)
R28	$N + NO_2 \rightarrow O + N_2O$	3×10^{-12}	(63)
R29	$N + NO_2 \rightarrow N_2 + O_2$	7×10^{-13}	(63)
R30	$N + NO_2 \rightarrow NO + NO$	2.3×10^{-12}	(63)
R31	$N + O_3 \rightarrow NO + O_2$	2×10^{-16}	(63)
Interactions between N_xO_y species and O_3			
R32	$NO_2 + N_2 \rightarrow NO + O + N_2$	$6.8\times10^{-6}(300/T_{gas})^2\exp(-36180/T_{gas})$	(63)
R33	$NO_2 + O_2 \rightarrow NO + O + O_2$	$0.78\times6.8\times10^{-6}(300/T_{gas})^2\exp(-36180/T_{gas})$	(63)
R34	$NO_2 + NO \rightarrow NO + O + NO$	$7.8\times6.8\times10^{-6}(300/T_{gas})^2\exp(-36180/T_{gas})$	(63)
R35	$NO_2 + NO_2 \rightarrow NO + O + NO_2$	$5.9\times6.8\times10^{-6}(300/T_{gas})^2\exp(-36180/T_{gas})$	(63)
R36	$NO + NO \rightarrow N + NO_2$	$3.3\times10^{-16}(300/T_{gas})^{0.5}\exp(-39200/T_{gas})$	(63)
R37	$NO + NO \rightarrow O + N_2O$	$2.2\times10^{-12}(300/T_{gas})^{0.5}\exp(-32100/T_{gas})$	(63)
R38	$NO + O_2 \rightarrow O + NO_2$	$2.8\times10^{-12}\exp(-23400/T_{gas})$	(63)
R39	$NO + NO_3 \rightarrow NO_2 + NO_2$	1.7×10^{-11}	(63)
R40	$NO_2 + NO_2 \rightarrow 2NO + O_2$	$3.3\times10^{-12}\exp(-13500/T_{gas})$	(63)
R41	$NO_2 + NO_3 \rightarrow NO + NO_2 + O_2$	$2.3\times10^{-13}\exp(-1600/T_{gas})$	(63)
R42	$NO_3 + M \rightarrow NO_2 + O + M$	$k_{R41}=3.1\times10^{-5}(300/T_{gas})^2\exp(-25000/T_{gas})$	
		M = N_2, O_2, NO	(63)
		$10\times k_{R41}$, M = N, O	
R43	$NO_3 + M \rightarrow NO + O_2 + M$	$k_{R42} = 6.2\times10^{-5}(300/T_{gas})^2\exp(-25000/T_{gas})$	
		M = N_2, O_2, NO	(63)
		$12\times k_{R42}$, M = N, O	
R44	$NO_3 + NO_2 \rightarrow NO + O_2 + NO_2$	$8.21\times10^{-14}\exp(-1480/T_{gas})$	(63)

R45	$O_2 + NO_2 \rightarrow NO + O_3$	$2.8\times10^{-12}\exp(-25400/T_{gas})$	(63)
R46	$NO_2 + O_3 \rightarrow O_2 + NO_3$	$1.2\times10^{-13}\exp(-2450/T_{gas})$	(63)
R47	$NO_3 + NO_3 \rightarrow O_2 + 2NO_2$	$4.3\times10^{-12}\exp(-3850/T_{gas})$	(63)
R48	$O_3 + M \rightarrow O_2 + O + M$	$6.3\exp(170/T_{gas}) \times 6.6\times10^{-10}\exp(-11600/T_{gas})$, M = N, O	(63)
		$0.38\times6.6\times10^{-10}\exp(-11600/T_{gas})$, $M = O_2$	(63)
		$6.6\times10^{-10}\exp(-11600/T_{gas})$ for the rest neutrals	(63)
R49	$NO_3 + NO_2 + M \rightarrow N_2O_5 + M$	$3.7\times10^{-30}(T_{gas}/298)^{-4.1}$	(63)
R50	$N_2O_5 + M \rightarrow NO_3 + NO_2 + M$	$1.33\times10^{-3}(T_{gas}/298)^{-4.1}\exp(-11000/T_{gas})$	(63)
R51	$NO_2 + NO_2 + M \rightarrow N_2O_4 + M$	$1.44\times10^{-33}(T_{gas}/298)^{-3.8}$	(63)
R52	$N_2O_4 + M \rightarrow NO_2 + NO_2 + M$	$1.33\times10^{-5}(T_{gas}/298)^{-3.8}\exp(-6400/T_{gas})$	(63)
R53	$NO + NO_2 + M \rightarrow N_2O_3 + M$	$3.26\times10^{-34}(T_{gas}/298)^{-7.7}$	(63)
R54	$N_2O_3 + M \rightarrow NO + NO_2 + M$	$2.01\times10^{-7}(T_{gas}/298)^{-8.7}\exp(-4880/T_{gas})$	(63)

‡ All 3-body reactions are in the unit of [$cm^6\ s^{-1}$]
§ Equation (s1)

Table S2. The assigned coefficient values of a_i for the equation S1in Kelvin (63).

$$E_v = 3395v[1 - 6.217 \times 10^{-2}(v+1)]$$

$$k_v(T)[cm^3s^{-1}] = \frac{(E_v + 3000)^{a_1}}{T^{a_2}} exp\left(a_3 + \frac{38370}{T}a_4 + \frac{E_v}{T}a_5\right)$$

v	a_1	a_2	a_3	a_4	a_5
0 ≤v≤ 8	-0.419312	-0.37836	-23.04468	-0.992436	0.989385
9 ≤v≤ 12	-3.42306	-1.4234	1.423118	-0.919692	0.917323
13 ≤v≤ 23	6.4805404	-0.279371	-96.75885	-0.037869	0.019647